Chinese Chemical Letters 36 (2025) 109882

Contents lists available at ScienceDirect

Chinese Chemical Letters

journal homepage: www.elsevier.com/locate/cclet

Insight into the activation of peroxymonosulfate by N-doped copper-based carbon for efficient degradation of organic pollutants: Synergy of nonradicals

Mengmeng Ao[a], Jian Wei[c], Chuan-Shu He[b], Heng Zhang[b], Zhaokun Xiong[b,*], Yonghui Song[a,c,*], Bo Lai[b]

[a] College of Environmental Sciences, Liaoning University, Shenyang 110036, China
[b] State Key Laboratory of Hydraulics and Mountain River Engineering, College of Architecture and Environment, Sichuan University, Chengdu 610065, China
[c] State Key Laboratory of Environmental Criteria and Risk Assessment, Chinese Research Academy of Environmental Sciences, Beijing 100012, China

ARTICLE INFO

Article history:
Received 19 January 2024
Revised 29 March 2024
Accepted 10 April 2024
Available online 10 April 2024

Keywords:
N-doped copper-based carbon
Phenolic compounds
Peroxymonosulfate
Nonradical pathway
Quantitative structure-activity relationship (QSAR)

ABSTRACT

The contamination of water resources by phenolic compounds (PCs) presents a significant environmental hazard, necessitating the development of novel materials and methodologies for effective mitigation. In this study, a metallic copper-doped zeolitic imidazolate framework was pyrolyzed and designated as Cu-NC-20 for the activation of peroxymonosulfate (PMS) to degrade phenol (PE). Cu-NC-20 could effectively address the issue of metal agglomeration while simultaneously diminishing copper dissolution during the activation of PMS reactions. The Cu-NC-20 catalyst exhibited a rapid degradation rate for PE across a broad pH range (3–9) and demonstrated high tolerance towards coexisting ions. According to scavenger experiments and electron paramagnetic resonance analysis, singlet oxygen ($^1O_2$) and high-valent copper-oxo (Cu(III)) were the predominant reactive oxygen species, indicating that the system was nonradical-dominated during the degradation process. The quantitative structure-activity relationship (QSAR) between the oxidation rate constants of various substituted phenols and Hammett constants was established. It indicated that the Cu-NC-20/PMS system had the optimal oxidation rate constant with σ^- correlation and exhibited a typical electrophilic reaction pattern. This study provides a comprehensive understanding of the heterogeneous activation process for the selective removal of phenolic compounds.

The environmental impact of phenolic compounds has become a growing concern in recent years. The discharge of phenolic compounds has not only degraded the quality of ecosystems but also poses a significant risk to ecological stability and human health, as outlined in key environmental studies [1]. Phenolic compounds, characterized as a prevalent group of organic pollutants that resisted biodegradation, were found extensively in various industries, agricultural practices, and medical facilities. The frequent presence of phenolic compounds in aquatic systems has been extensively documented [2]. While these compounds have been instrumental in supporting the trajectory of rapid economic development, their adverse environmental effects have not gone unnoticed [3]. Notably, inherent high toxicity, resistance to natural degradation processes, and potential for bioaccumulation of phenolic compounds posed a dual threat: toxic and potentially carcinogenic to aquatic life and humans, even at low concentrations [4]. In light of these concerns, the advancement of effective technologies for the removal and complete mineralization of phenolic compounds from aquatic environments is crucial in promoting environmental sustainability.

Among state-of-the-art wastewater treatment methodologies, advanced oxidation processes (AOPs) have emerged as pivotal techniques in decontaminating water resources for refractory pollutants. Within this spectrum, peroxymonosulfate (PMS) stands out as an oxidant that aligns with environmental sustainability and cost-effectiveness, distinguished by its solubility and stability in aqueous solutions. The activation of PMS is characterized by a diverse array of reaction pathways, which include both radical-driven and non-radical processes [5]. The conventional radical pathway predominantly involves the formation of hydroxyl radicals ($^{\bullet}OH$) and sulfate radicals ($SO_4^{\bullet-}$). However, challenges arise in practical water treatment scenarios due to complex water matrices, which can adversely affect the catalytic effectiveness. Specifically, the produced $^{\bullet}OH/SO_4^{\bullet-}$ tend to react with coexisting substances like

* Corresponding authors.
E-mail addresses: scuxzk@scu.edu.cn, scuxzk@163.com (Z. Xiong), songyh@creas.org.cn (Y. Song).

https://doi.org/10.1016/j.cclet.2024.109882
1001-8417/

inorganic iron and natural organic matter (NOM), leading to less potent oxidation by-products such as $Cl_2^{\bullet-}$ and $CO_3^{\bullet-}$, thereby hindering their broader application [6]. In contrast, the non-radical pathways, encompassing processes like surface activation complexes, electron transfer, and the involvement of high-valent species and singlet oxygen ($^1O_2$), offer a balanced approach with moderate oxidation capabilities. These pathways demonstrate selectivity in contaminant degradation with a high level of resistance to typical radical quenchers, and maintain effectiveness across diverse pH conditions [7]. Recent studies have increasingly focused on the role of high-valent metals in degrading pollutants, particularly through the activation of persulfates. Notably, copper in its high-valent state, Cu(III), which demonstrates a redox potential of 2.3 V for the Cu(III)/Cu(II) couple, has been observed to possess slightly higher effectiveness in comparison to other high-valent metals such as iron (with a redox potential of 2.2 V) and manganese (exhibiting a redox potential of 1.68 V) [8]. This underscores the potential of designing hetero-copper-based catalysts to optimize PMS activation to facilitate the production of Cu(III). This approach is positioned as a forward-looking strategy in the realm of water treatment technologies.

Metal-organic frameworks (MOFs) consist of nodes containing metal elements and are interconnected by organic linkers [9]. Their expansive surface area, coupled with a finely tuned microporous structure and well-organized morphology, positions them as potential substitutes for conventional heterogeneous catalysts in environmental clean-up efforts [10]. Moreover, MOFs-derived carbon materials not only retain the framework of MOFs but also exhibit enhanced stability and electrical conductivity, and are widely investigated for the activation of PMS [11–13]. Specifically, zeolitic-imidazolate frameworks (ZIFs) with unique topology and versatility in different metal centers are the most widely used precursors for the preparation of nitrogen-doped carbon.

Therefore, we synthesized copper-based N-doped carbon (Cu-NC-20) by *in situ* doping of metallic copper in ZIF-8 and pyrolyzed under argon atmosphere. The research provided a new pathway for PMS activation with excellent degradation performance towards phenol (PE). Detailed analyses of the catalysts' morphology and surface characteristics were performed using a range of characterization techniques. In this research, essential reaction variables, such as namely initial pH, catalyst quantity, PMS concentration, and PE levels, were comprehensively explored. The predominant ROS in the Cu-NC-20/PMS system, identified as $^1O_2$ and Cu(III), were pinpointed through scavenging experiments, EPR analysis, and *in-situ* Raman spectroscopic techniques. Furthermore, the influence of coexisting ions and the impact on PE degradation in actual water samples were investigated, alongside evaluating the catalyst's recyclability for practical use. Most notably, the degradation behaviors of seven selected phenolic compounds were analyzed by QSAR. This provided insights into the selective oxidation capabilities of the Cu-NC-20/PMS system, particularly in relation to Hammett constants.

Comprehensive investigations into the morphological characteristics of the materials, both prior to and following the pyrolysis process, were conducted. These analyses employed scanning electron microscopy (SEM) and transmission electron microscopy (TEM) techniques. Initial observations, as depicted in Fig. S1 (Supporting information), indicated that the Cu-ZIF-20 samples were characterized by a distinct rhombic dodecahedral geometry, with the particle sizes predominantly falling within the 50–60 nm range. However, a significant transformation was observed post-pyrolysis treatment, conducted at a temperature of 900 °C. This change, displayed in Fig. 1a, manifested as a notable decrease in particle size and an overall collapse in the structural integrity of the Cu-NC-20. This phenomenon was likely a consequence of the disintegration of the organic components within the framework during the high-temperature pyrolysis [14,15]. Further detailed analysis using TEM and high-resolution TEM (HRTEM), as showcased in Figs. 1b and c, revealed a lack of extensive lattice fringes, thereby indicating the absence of highly crystalline structures of copper within the Cu-NC-20. In addition, the uniform distribution of various elements such as C, N, O, and Cu in the catalyst was confirmed through energy-dispersive X-ray spectroscopy (EDS) elemental mapping (Fig. 1d), and corresponding contents were listed in Table S1 (Supporting information). The technique EDS provided a clear visualization of the elemental composition and indicated the homogeneity of C, N, O, and Cu. N_2 adsorption-desorption tests showed that the BET surface area of N-C, Cu-NC-10, Cu-NC-20 and Cu-NC-40 was 972.23, 1127.54, 1169.84 and 1002.27 m^2/g, respectively (Fig. 1e). Comparison of Fig. S2 (Supporting information) and Fig. 1a revealed that the catalyst particle size became smaller and more pores after metal doping, so the specific surface area increased with the increase of copper doping, but the difference in BET with the change of copper content was not significant. Fig. S3 (Supporting information) showed the pore size distribution in the range of 0.75–2.00 nm. The above results demonstrated that catalysts with large specific surface areas and microporous structure helped to promote mass transfer between pollutant and oxidant molecules.

X-ray diffraction (XRD) patterns were performed to examine the crystal structure of catalysts. As depicted in Fig. S4 (Supporting information), only two peaks ($2\theta = 25.7°$ and 43.5°) belonging to the (002) and (101) crystalline facets of graphitic carbon were found for all catalysts, suggesting that all catalysts were successfully converted to amorphous carbon from ZIF-8-derived precursors after pyrolysis. The introduction of a minimal quantity of copper into the samples did not lead to any discernible alterations in their crystalline structure, and there were no oxide crystalline facets in the structure. Furthermore, the extent of graphitization in these samples was assessed using Raman spectroscopy. As depicted in Fig. S5 (Supporting information), the Raman spectra exhibited two prominent peaks at 1338 cm^{-1} (D band) and 1590 cm^{-1} (G band), as indicative vibrations of sp^2-bonded carbon atoms and structural defects, respectively [16–18]. Notably, the relative intensity ratio (I_D/I_G) remained relatively unchanged, suggesting that the incorporation of metallic copper did not significantly impact the degree of graphitization and the degree of defects in the material. The surface chemistry attributes of various samples were further analyzed using Fourier-transform infrared spectroscopy (FTIR), as shown in Fig. 1f. In this study, the FTIR spectroscopy results, aligning with the observations from XRD and Raman spectroscopy, indicated no significant changes were observed as the amount of Cu doping varied. The FTIR spectra exhibited a characteristic absorption band in the 3100 cm^{-1} to 3600 cm^{-1} regions. This specific band was interpreted as indicative of the stretching vibrations associated with hydroxyl (O–H) and amine (N–H) functional groups [19,20]. In the spectrum, the absorption range between 1200 cm^{-1} and 1660 cm^{-1} was attributed to the presence of nitrogen heteroatoms integrating into the sp^2 hybridized carbon lattice and the presence of C=C/C=O [21,22]. Additionally, the presence of a distinct absorption band in the 550-620 cm^{-1} region was identified as corresponding to the vibrational bonding patterns of Cu–N [23]. To further probe the surface chemical composition and the specific elemental states within the catalysts, X-ray photoelectron spectroscopy (XPS) was employed. The detailed analysis of the high-resolution N 1s spectrum for the Cu-NC-20 sample revealed the presence of three distinct peaks as depicted in Fig. 1g. These peaks were classified as graphitic nitrogen at 401.03 eV, pyrrolic nitrogen at 399.77 eV, and pyridinic nitrogen at 398.45 eV. The latter, observed at 398.45 eV, was hypothesized to be closely associated with the bonding configurations involving Cu-N interactions [24]. Despite the subtle differences in binding energies made it

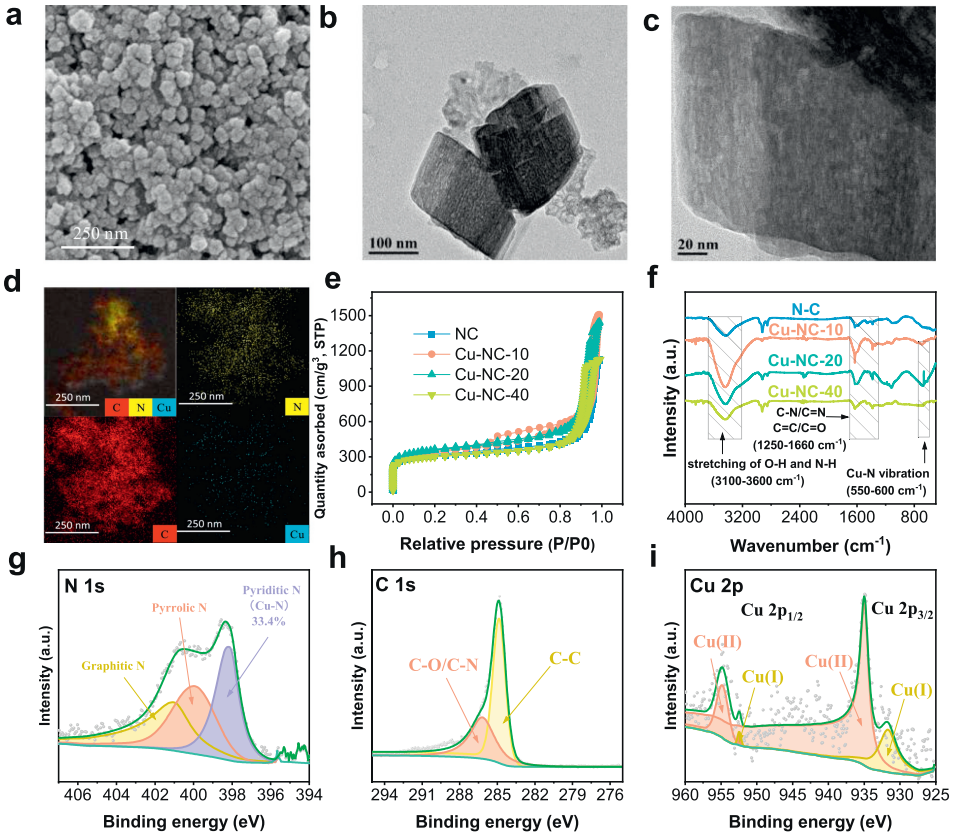

Fig. 1. SEM images of (a) Cu-NC-20 and (b, c) TEM of Cu-NC-20. (d) Elemental mapping images of Cu-NC-20. (e) N_2 adsorption-desorption isotherms and (f) FTIR spectra of samples. XPS fitting results of (g) N 1s, (h) C 1s and (i) Cu 2p.

challenging to distinctly identify Cu-N, the presence of Cu–N was further supported by the peaks in the 550–600 cm^{-1} range in the FTIR spectrum (Fig. 1f). The high-resolution C 1s spectrum, shown in Fig. 1h, was divided into two peaks corresponding to C–C (284.8 eV) and C-N/C–O (286.1 eV) bonds [25,26]. The Cu 2p high-resolution spectra in Fig. 1i revealed two primary peaks at 934.8 and 954.3 eV, identified as Cu 2p$_{3/2}$ and Cu 2p$_{1/2}$, respectively, indicating the presence of copper in both Cu(II) and Cu(I) valence states, with contents of 86% and 14%, respectively (Fig. S13 in Supporting information). Collectively, these findings confirmed the successful synthesis of metallic copper-doped zeolitic imidazolate framework derivatives.

Experimental observations illustrated in Fig. 2a indicate that using PMS alone had a minimal impact on phenol (PE) removal, accounting for less than 5% reduction. This suggested that PMS lacked substantial oxidizing capability for PE degradation, despite its high redox potential. Additionally, as shown in Fig. S6 (Supporting information), all tested catalysts demonstrated limited adsorption efficiency towards PE, the maximum adsorption rate did not exceed 30%. Fig. 2b highlighted that the degradation rate was also only 38% after the addition of N-C without Cu atoms, and the addition of copper significantly enhanced the catalytic performance. Notably, Cu-NC-20 achieved complete degradation of PE within 10 min, exhibited the fastest kinetic rate constant (0.544 min^{-1}) and the highest TOC removal rate (66%), and utilized nearly 100% of the PMS within the same duration (Figs. S7 and S14 in Supporting information). In addition, the reaction rate (KMCP, divide k_{obs} by the content of metal, dosage of catalyst, and PMS) values of Cu-NC-20 were much higher than those of state-of-the-art heterogeneous catalysts reported recently (Fig. 2c and Table S2 in Supporting information). Consequently, Cu-NC-20 was identified as the optimal catalyst with a maximum value of k_{obs}. To explore the copper

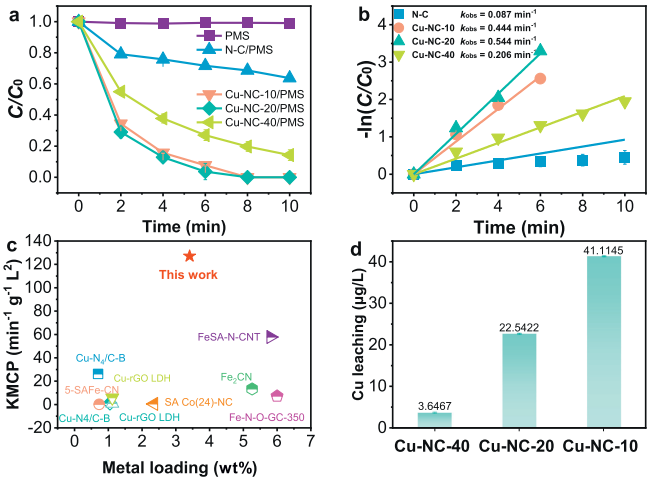

Fig. 2. (a) The removal efficiency and (b) corresponding k_{obs} of different catalysts, (c) comparison of KMCP values of different systems, (d) Cu leaching. Reaction condition: [PE] = 5 mg/L, [PMS] = 0.25 mmol/L, [catalyst] = 70 mg/L.

ion leaching of different catalysts, shown in Fig. 2d, the addition of copper did lead to an increase in leaching. Moreover, the leached copper ions from Cu-NC-20 were measured at only 23 μg/L, which was significantly below the maximum permissible limit of 1.0 mg/L set by the Sanitary Standard for Drinking Water in China (GB5749–2006).

A comprehensive study was conducted to assess the influence of various operational parameters on PE degradation within the Cu-NC-20/PMS system. These parameters included the quantities of catalyst and PMS, the pH value, and the PE concentration. As

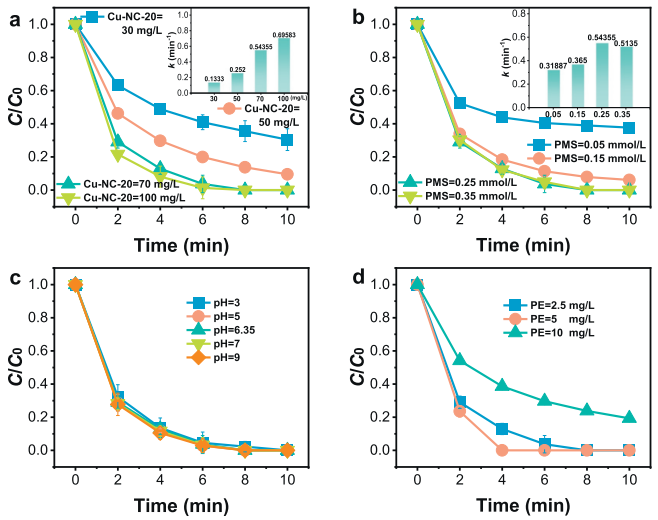

Fig. 3. Influence of (a) catalyst amount, (b) PMS quantity, (c) pH levels, and (d) PE concentrations on PE degradation through Cu-NC-20/PMS. Reaction conditions: [PE] at 5 mg/L for (a), (b), (c); [PMS] at 0.25 mmol/L for (a), (c), (d); catalyst presence at 70 mg/L for (b), (c), (d).

illustrated in Fig. 3a, an increase in the concentration of Cu-NC-20 from 30 mg/L to 100 mg/L was found to enhance the degradation efficiency markedly, from 76.0% to a complete 100% within 10 min. This enhancement in efficiency can be largely attributed to the increased availability of active sites for the activation of PMS, leading to a higher generation rate of reactive species with elevated catalyst concentrations. Nevertheless, the increment in catalyst dosage from 70 mg/L to 100 mg/L did not show a proportional increase in efficiency, which could be due to the limitations in diffusion arising from an overabundance of the catalyst in the system [27,28]. Consequently, 70 mg/L was identified as the optimal catalyst dosage for further experiments, because of balancing efficiency and cost considerations. The role of PMS concentration was also critical, as a primary source of active species in the degradation process. The increase of PMS concentration from 0.05 mmol/L to 0.25 mmol/L expedited PE degradation, as shown in Fig. 3b. However, elevating the PMS concentration to 0.35 mmol/L did not yield further improvement, possibly due to saturation of the activation sites [29,30]. Consequently, an optimal concentration of 0.25 mmol/L for PMS was established. The effectiveness of Fenton and Fenton-like processes was well-known to be heavily influenced by pH levels, presenting challenges for their widespread practical use. This sensitivity has made the regulation of pH a critical aspect in applications involving persulfate activation [31,32]. The influence of pH in Cu-NC-20/PMS system was investigated in Fig. 3c. The high efficiency in PE removal across a broad pH spectrum ranging from 3 to 9 was remarkable. It was noteworthy that there was no significant variance in the removal efficiency between acidic and alkaline environments. This makes the Cu-NC-20/PMS system have a wide range of prospects in practical applications. Additionally, as illustrated in Fig. 3d, while an increase in PE concentration slightly reduced the degradation rate, the system still achieved an impressive 84.2% removal efficiency at a PE concentration of 10 mg/L.

In the Cu-NC-20/PMS reaction system, two specific radical scavengers, MeOH and TBA, were employed to investigate the potential involvement of $SO_4^{\bullet-}$ and $^{\bullet}OH$. Detailed rate constants, provided in Table S3 (Supporting information), revealed MeOH could quench both types of radicals, whereas TBA showed a preferential affinity for quenching $^{\bullet}OH$ only. Experimental data presented in Figs. 4a and b demonstrated that even significant variations in the ratios of MeOH and TBA, from 100:1 to 1000:1, did not markedly alter the degradation efficiency of PE. This outcome implied that neither $SO_4^{\bullet-}$ nor $^{\bullet}OH$ radicals played a major role in the degradation process within Cu-NC-20/PMS system. Furthermore, SOD and BQ were introduced as probes to investigate the presence of $O_2^{\bullet-}$ radicals. As indicated in Fig. 4c and Fig. S8 (Supporting information), the negligible impact of these scavengers suggested that $O_2^{\bullet-}$ was not a predominant reactive oxygen species in the reaction milieu. Complementing these findings, an EPR study utilizing DMPO as a trapping agent was conducted. The results showed an absence of typical signals associated with DMPO-$^{\bullet}OH$ or DMPO-$SO_4^{\bullet-}$ adducts (Fig. 4d). Instead, the dominant presence of a DMPOX signal was noted, which was indicative of the rapid oxidation of DMPO. This observation lent support to the hypothesis that non-radical mechanisms might be significantly contributing to the overall reaction process in the Cu-NC-20/PMS system.

Previous studies had reported that $^1O_2$ was generated during PMS activation, and the role of $^1O_2$ was explored using furfuryl alcohol (FFA) as the quenching agent. As displayed in Fig. 4e, the addition of FFA effectively suppressed the degradation of PE and the suppression was found to be enhanced with the increase in FFA concentration. The addition of both sodium azide (NaN_3) and L-histidine to the system showed a strong inhibition [33]. Observable suppressive effects were recorded in the Cu-NC-20/PMS system with the addition of NaN_3 and L-histidine, as illustrated in Fig. S9a (Supporting information). This addition led to a noticeable reduction in the system's efficiency for degrading PE. Furthermore, as depicted in Fig. S9b (Supporting information), the degradation of PE in the Cu-NC-20/PMS system was more effective in D_2O than in H_2O. This enhancement in D_2O suggested an elevated effectiveness of the system, largely driven by the activity of $^1O_2$. The findings collectively highlighted the crucial role of $^1O_2$ in the degradation process within the Cu-NC-20/PMS system. The EPR spectrum of Fig. 4f showed the appearance of a similar three-line signal (1:1:1) for the TEMPN adduct, and no significant signal was detected by only PMS. Notably, the TEMPN signal intensity increased significantly with increasing reaction time, indicating that Cu-NC-20 could activate PMS to generate $^1O_2$.

Recent advancements in the field have highlighted catalyst-mediated organic contaminant degradation *via* direct electron transfer mechanisms, bypassing the need for ROS involvement [34]. Consequently, this underscored the importance of investigating the presence and efficacy of electron transfer pathways specifically in the Cu-NC-20/PMS system. It was assumed that organic contaminants could be transferred to sub-stable complexes through the catalyst and PMS, leading to the degradation of contaminants. PMS remained stable in catalyst solutions without organic contaminants, but when organic contaminants were introduced, PMS decomposed to degrade the contaminants. That indicated the organic contaminant was the initiator of PMS activation [35,36]. An analysis was carried out to assess the impact of combining Cu-NC-20 with PMS before the treatment of PE. As indicated in Fig. 5a, premixing these two components led to a noticeable reduction in the effectiveness of the PE oxidation process. This reduction became more pronounced with an increase in the premixing duration, suggesting that the role of PMS in degrading PE was predominantly through the activation of the catalyst. Concurrently, the depletion of PMS in the Cu-NC-20 system was investigated, both in the presence and absence of PE. Fig. S10 (Supporting information) illustrated that the PMS concentration declined at a similar rate irrespective of the presence or absence of PE. These findings collectively implied that the conventional electron transfer mechanism was not the predominant pathway in the Cu-NC-20/PMS system.

Additionally, a chronoamperometry experiment was conducted to delve into the activation dynamics of PMS in the presence of the Cu-NC-20 catalyst. The results, depicted in Fig. 5b, showed a

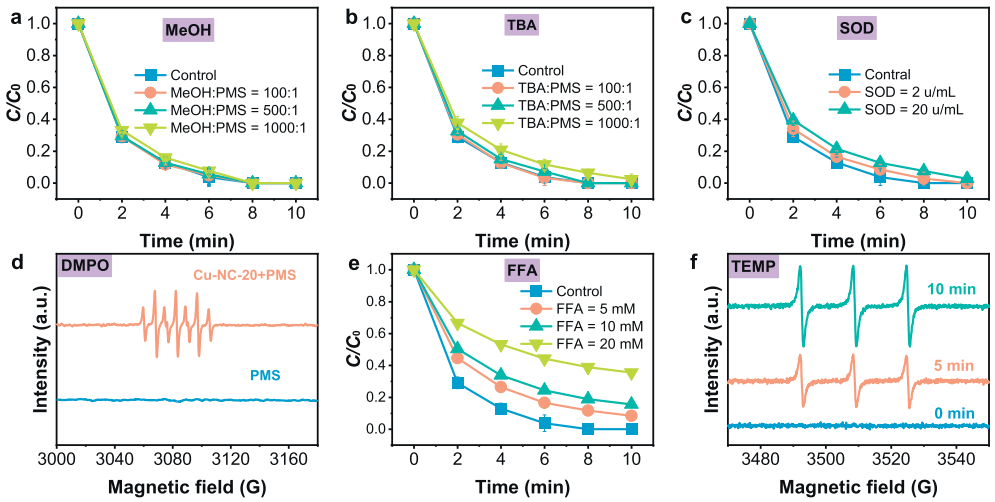

Fig. 4. Impact of varying concentrations of (a) MeOH, (b) TBA, (c) SOD on PE degradation, (d) EPR spectra in Cu-NC-20/PMS, DMPO as trapping agent, (e) influence of varied FFA concentrations on PE degradation, (f) EPR spectra in Cu-NC-20/PMS, TEMP as trapping agent. Reaction conditions: [PE] at 5 mg/L, [PMS] at 0.25 mmol/L, catalyst presence at 70 mg/L, [DMPO] at 20 mmol/L, [TEMP] at 20 mmol/L.

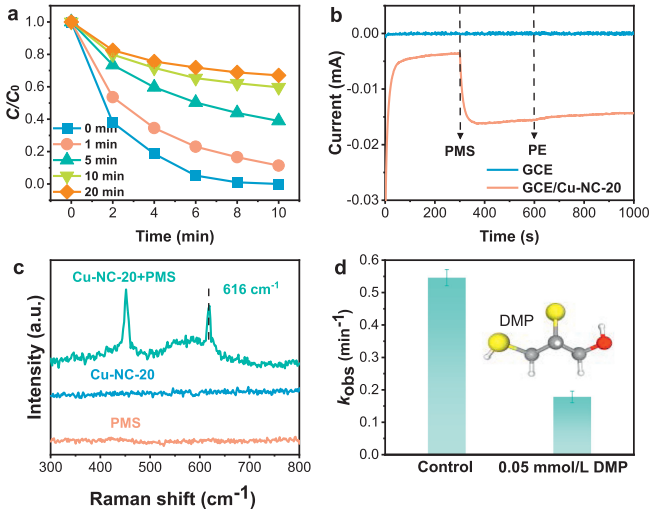

Fig. 5. (a) The degradation efficiency of PE after premixing Cu-NC-20 with PMS, (b) the amperometric *i-t* curve of the reaction at 0.0 V, (c) the *in-situ* Raman patterns of Cu-NC-20, (d) and the k_{obs} of adding DMP in the Cu-NC-20/PMS system. Reaction conditions: [PE] = 5 mg/L, [PMS] = 0.25 mmol/L, catalyst = 70 mg/L, [DMP] = 0.05 mmol/L.

notable change in the current immediately following the introduction of PMS under open circuit conditions. This change was indicative of an effective electron transfer process occurring between Cu-NC-20 and PMS. It was reported in the literature that transition metal catalytic systems could form high-valent intermediates by heterolytic perovskite O-O bonding. Electron transition from Cu-NC-20 to PMS was instrumental in the generation of high-valent copper-oxygen species [Cu(III)-OH], a process initiated by the heterolytic cleavage of O-O bonds, which subsequently led to the activation of PMS, as mentioned in reference [37]. To validate the formation of high-valent copper, Raman spectroscopy was employed. As shown in Fig. 5c, an emergent peak around 616 cm^{-1} in the Cu-NC-20/PMS system was observed, which was likely representative of high-valent copper-oxo species. This assumption was based on the peak's alignment with the known Cu-O stretch vibration peak characteristic of Cu(III). Further evidence of Cu(III) presence was deduced by employing 2,3-dimercapto-1-propanol (DMP) as a chelating agent. DMP was recognized for its affinity to bind copper sites, subsequently inhibiting their activity by forming robust

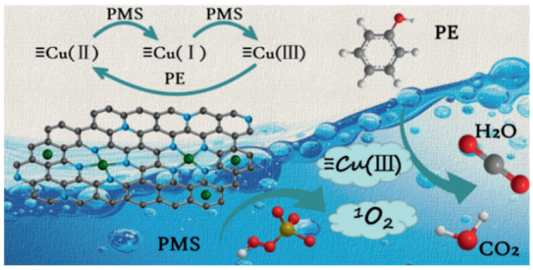

Fig. 6. The mechanism for the PE removal in Cu-NC-20/PMS system.

complexes with sulfhydryl groups without depleting PMS (Fig. S11 in Supporting information). The substantial reduction in k_{obs} observed in Fig. 5d upon the addition of 0.05 mmol/L DMP to the Cu-NC-20/PMS system, further corroborated the presence of Cu(III) species in the system [38].

Drawing from the experimental findings and subsequent analysis, a proposed mechanism for the degradation of PE by the Cu-NC-20/PMS system was developed. This mechanism predominantly involved $^1O_2$ and Cu(III) species, as illustrated in Fig. 6. The process initiated with the coordination of Cu(II) with PMS, forming a Cu(II)–PMS complex. This complex underwent an electron transfer, reducing Cu(II) to Cu(I) (Eq. 1). Subsequently, Cu(I) interacted with PMS in a double electron transfer reaction to form Cu(III) (Eq. 2) [39]. Upon the adsorption of PE onto Cu-NC-20, Cu(III) was reverted to Cu(II) through an electron transfer step (Eq. 3), concurrently leading to the degradation of PE into smaller molecules. The activation of PMS by Cu-NC-20 was accompanied by the formation of $SO_5^{\bullet-}$, which further generated $^1O_2$. In this process, Cu-NC-20 served as an electron transfer mediator, facilitating the electron movement from PE molecules to PMS, thereby expediting the production of $^1O_2$ (Eq. 4) [40,41]. Consequently, PE was broken down into mineralized small molecules through a combined action of Cu(III) and $^1O_2$ in a non-radical electron transfer process (Eqs. 3 and 5).

$$\equiv Cu(II) + HSO_5^- \rightarrow \equiv Cu(II) - HSO_5^- \rightarrow \equiv Cu(I) + SO_5^{\bullet-} + H^+ \quad (1)$$

$$\equiv Cu(I) + HSO_5^- \rightarrow \equiv Cu(III)OOSO_3 + SO_4^{2-} + OH^- \quad (2)$$

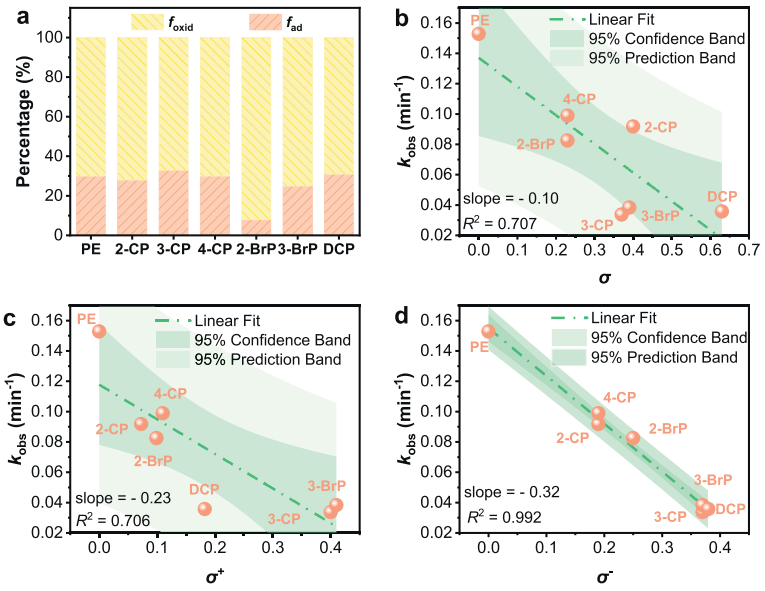

Fig. 7. (a) The fractions of different PCs in Cu-NC-20/PMS system of two fractions: adsorbed fraction (f_{ad}) and oxidation fraction (f_{aq}). Correlation of reaction rate constants (k_{obs}) for substituted phenols oxidation by Cu-NC-20/PMS system to the (b) Hammett σ constant, (c) Hammett σ^+ constant and (d) Hammett σ^- constant. Reaction conditions: [PCs] = 5 mg/L, [PMS] = 0.25 mmol/L, catalyst = 70 mg/L.

$$\equiv \mathrm{Cu(III)} + \mathrm{PE} \rightarrow \equiv \mathrm{Cu(II)} + \mathrm{products} \quad (3)$$

$$\mathrm{SO_5^{\bullet -}} + \mathrm{H_2O} \rightarrow \mathrm{HSO_4^-} + {}^1\mathrm{O_2} \quad (4)$$

$${}^1\mathrm{O_2} + \mathrm{PE} \rightarrow \mathrm{CO_2} + \mathrm{H_2O} + \mathrm{products} \quad (5)$$

Previous studies have reported that the ability of non-radical systems to remove pollutants may depend on the electronic nature of the pollutants with some selectivity. Therefore, we carried out a more in-depth study of the oxidation rate of phenolic compounds by Cu-NC-20/PMS with its structural characterization by QSAR. For this purpose, the study incorporated the use of Hammett constants (σ, σ^+, and σ^-). These constants were paramount in physical organic chemistry, serving as robust descriptors for substituent effects. They offered a comprehensive quantitative analysis to characterize the electron-donating or electron-withdrawing nature of substituents through their numerical values. Meanwhile, large negative values indicated strong electron-donating characteristics and large positive values signified potent electron-withdrawing capacity. This investigative approach led to an in-depth examination of the oxidation rates of a series of substituted phenols, specifically including 2-chlorophenol (2-CP), 3-chlorophenol (3-CP), 4-chlorophenol (4-CP), 2-bromophenol (2-BrP), 3-bromophenol (3-BrP), and 2,4-dichlorophenol (DCP). These compounds were selected to represent a diverse range of structural variations, and their degradation behaviors in the Cu-NC-20/PMS system were meticulously analyzed to establish a clear correlation between molecular structure and oxidative reactivity.

Fig. 7a presented the adsorption and degradation rates of various phenolic compounds in the Cu-NC-20/PMS system at a uniform reaction time of 10 min. For a clearer understanding of the QSAR, the contribution of adsorption to the degradation process was separated, and the remaining degradation rates were then analyzed in relation to the Hammett constant. As depicted in Figs. 7b-d, the negative Hammett constant (σ^-) showed the strongest correlation with the oxidation of phenolic compounds by the Cu-NC-20/PMS system, evidenced by an R^2 value of 0.992. This correlation revealed that the rate of oxidation decreased as the σ^- increased. The negative trend of this relationship indicated that the Cu-NC-20/PMS system demonstrated higher reactivity towards phenolic compounds that possessed electron-donating groups, a characteristic common in electrophilic reactions [42,43].

A detailed study was conducted to critically evaluate the effect of potential interfering factors in the natural aqueous environment on Cu-NC-20/PMS. This study focused on how the presence of ubiquitous inorganic anions and natural organic matter (NOM) affects the degradation efficiency of PE in the Cu-NC-20/PMS system. Specifically, the study explored the influence of prevalent inorganic ions such as Cl^-, HPO_4^{2-}, HCO_3^- and humic acid (HA). The experimental data revealed a negligible influence of these substances on the PE degradation process (Fig. 8a). This observation led to the inference that $SO_4^{\bullet -}$ and $^{\bullet}OH$ might not play a significant role in the catalytic mechanism of this system. The results indicated that the degradation process predominantly proceeded *via* non-radical pathways, showing a notable resistance to the influence of coexisting inorganic anions. Further, to evaluate the practical applicability of the Cu-NC-20 catalyst in real-world scenarios, experiments were performed using tap water and surface water as testing media. As illustrated in Fig. 8b, the experiments demonstrated high efficacy in PE removal, achieving complete removal in tap water (100%) and near-complete removal in surface water (95%). These results highlighted the potential of the Cu-NC-20/PMS system for effective treatment of PE in diverse natural water sources. Additionally, the recyclability of the Cu-NC-20 catalyst was examined to gauge its sustainability and practical utility. The decline in the catalyst's efficiency was indicated in Fig. 8c, with the degradation rate of PE dropping to 50% by the third cycle of usage. An in-depth analysis was conducted to understand the cause of this decrease in performance. N 1s XPS spectra comparisons of Cu-NC-20, before and after the reactions, showed a reduction in the Cu-N content from 33.4% to 23.8%. This reduction highlighted the loss of active catalytic sites as a primary factor for the observed decrease in performance (Fig. 1g and Fig. S12 in Supporting information). To counteract this, the catalyst underwent re-calcination after the third cycle. Post re-calcination, an increase in the Cu-N content to 29.6% was observed in the fourth and fifth cycles, as shown in Fig. 8d. This recovery process restored the efficiency of the catalyst and enabled

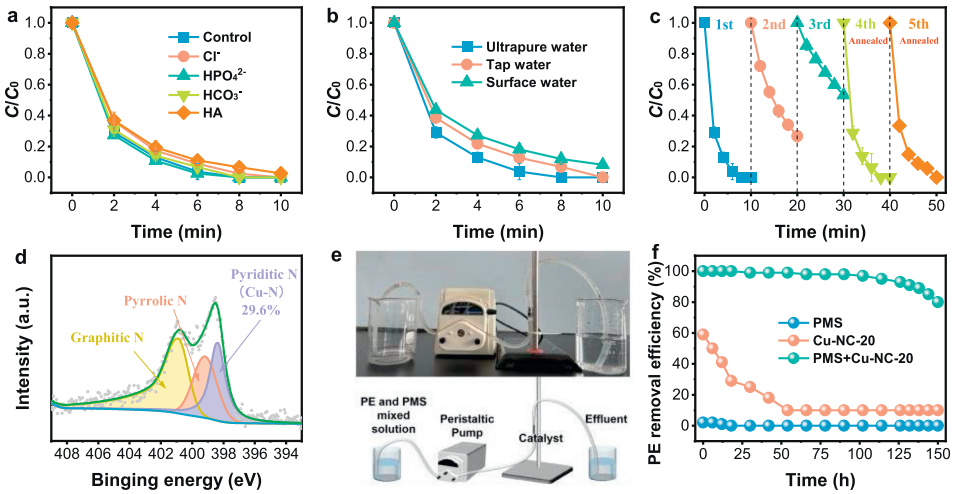

Fig. 8. (a) Impact on PE degradation by different inorganic anions, HA, (b) PE removal rates in ultrapure, surface water, (c) Cu-NC-20 reusability for PE, (d) XPS analysis post-regeneration, (e) schematic representation, (f) PE removal rates in Cu-NC-20/PMS systems. Reaction conditions: [PE] = 5 mg/L, [PMS] = 0.25 mmol/L, catalyst = 70 mg/L.

Cu-NC-20 to degrade 100% of PE within 10 min in subsequent cycles. This recovery of activity affirmed the pivotal role of Cu-N sites in catalysis and underscored the Cu-NC-20/PMS system's adaptability and recyclability for real-world application. Collectively, these findings underscored the broad applicability and remarkable recovery potential of the Cu-NC-20/PMS process for water treatment.

To further assess the recyclability and practical utility of the catalyst, a continuous flow reactor was designed, drawing upon methodologies outlined in references [44–46]. This reactor was constructed by embedding 20 mg of the Cu-NC-20 catalyst into a cotton matrix. The reactor was then employed in a top-to-bottom flow configuration, where a mixture of PE and PMS was continuously fed into it (Fig. 8e). The hydrodynamic residence time (HRT) in this setup was maintained at 14.4 min. The efficiency of the reactor in processing simulated PE wastewater was demonstrated in Fig. 8f. It was observed that the removal efficiency of PE using either PMS or Cu-NC-20 alone was below 20%. In stark contrast, the combined Cu-NC-20/PMS system exhibited a removal efficiency exceeding 90%. However, a noticeable decrease in efficiency was recorded after 100 h of operation. Notably, the concentration of PMS utilized in the continuous flow setup was lower (0.15 mmol/L) compared to that used in beaker experiments (0.25 mmol/L). This reduction, alongside the constant catalyst amount, highlighted the effectiveness and advantages of Cu-NC-20 in a continuous flow scenario and underscored its potential for real-world water treatment applications.

In this study, we prepared a copper-based nitrogen-doped carbon material that showed excellent catalytic performance in complete PE degradation with k_{obs} (0.544 min^{-1}) was 7 times higher than that of the catalyst without added metal (0.087 min^{-1}). The effects of pH, the concentration of catalyst, PMS, and PE on the activation of the Cu-NC-20/PMS system were explored. Through quenching experiments and EPR analyses, it was finally determined that the main reactive ROS for the degradation process of the system were $^1O_2$ and Cu(III). Therefore, it showed stable degradation ability in the investigation of the effects of inorganic anions and NOM. Besides, the QSAR between the phenolic oxidation rate and Hammett constant in the Cu-NC-20/PMS system indicated that the high selectivity of the system for phenolic compounds was highly dependent on its substituent species. Overall, the insights gained in this study contributed to the understanding of the design principles of Cu-based nitrogen-doped carbon catalysts. These findings were valuable for the efficient and selective degradation of phenolic compounds by PMS-based AOPs.

Declaration of competing interest

The authors declare that they have no known competing financial interests or personal relationships that could have appeared to influence the work reported in this paper.

CRediT authorship contribution statement

Mengmeng Ao: Writing – original draft, Writing – review & editing, Conceptualization, Formal analysis, Investigation. **Jian Wei:** Data curation, Methodology, Software. **Chuan-Shu He:** Methodology, Software. **Heng Zhang:** Methodology, Software. **Zhaokun Xiong:** Conceptualization, Funding acquisition, Project administration, Supervision, Validation, Writing – original draft, Writing – review & editing. **Yonghui Song:** Funding acquisition, Project administration, Supervision, Visualization. **Bo Lai:** Funding acquisition, Project administration, Supervision.

Acknowledgments

The authors would like to acknowledge the financial support from Sichuan Program of Science and Technology (No. 2021ZDZX0012) and the National Natural Science Foundation of China (No. 52200105).

Supplementary materials

Supplementary material associated with this article can be found, in the online version, at doi:10.1016/j.cclet.2024.109882.

References

[1] E. Mousali, M.A. Zanjanchi, Reac. Kinet. Mech. Cat. 130 (2020) 547–566.
[2] L. Gnanasekaran, S. Rajendran, A.K. Priya, et al., Environ. Res. 195 (2021) 110852.
[3] H. Singer, S. Müller, C. Tixier, et al., Environ. Sci. Technol. 36 (2002) 4998–5004.
[4] F. Wang, J. Xu, Z. Wang, et al., Appl. Catal. B 312 (2022) 121438.
[5] J. Lee, U. von Gunten, J.H. Kim, Environ. Sci. Technol. 54 (2020) 3064–3081.
[6] X. Li, J. Ma, Y. Gao, et al., Chem. Eng. J. 427 (2022) 131995.
[7] J. Dong, W. Xu, S. Liu, et al., J. Cleaner Prod. 321 (2021) 128781.
[8] Y. Liu, W. Miao, Y. Feng, et al., J. Hazard. Mater. 403 (2021) 123691.
[9] Q. Yang, Q. Xu, H.L. Jiang, Chem. Soc. Rev. 46 (2017) 4774–4808.
[10] X. Li, Z. Ao, J. Liu, et al., ACS Nano 10 (2016) 11532–11540.
[11] M. Hao, M. Qiu, H. Yang, et al., Sci. Total Environ. 760 (2021) 143333.
[12] B. Huang, Z. Wu, X. Wang, et al., Environ. Sci. Technol. 57 (2023) 15667–15679.
[13] Z. Wu, B. Huang, X. Wang, et al., Environ. Sci. Technol. 57 (2023) 14046–14057.

[14] Y. Wang, J.Le Roux, T. Zhang, et al., Environ. Sci. Technol. 48 (2014) 14534–14542.
[15] Y. Deng, Y. Dong, G. Wang, et al., ACS Appl. Mater. 9 (2017) 9699–9709.
[16] A. Sadezky, H. Muckenhuber, H. Grothe, et al., Carbon 43 (2005) 1731–1742.
[17] Z. Wu, Z. Xiong, R. Liu, et al., J. Hazard. Mater. 427 (2022) 128204.
[18] Y. Shang, Y. Kan, X. Xu, Chin. Chem. Lett. 34 (2023) 108278.
[19] C. Liu, H. Dai, C. Tan, et al., Appl. Catal. B 310 (2022) 121326.
[20] X. Wang, Z. Xiong, H. Shi, et al., Appl. Catal. B 329 (2023) 122569.
[21] Y. Wang, H. Sun, H.M. Ang, et al., J. Colloid Interface Sci. 433 (2014) 68–75.
[22] B. Huang, X. Ren, J. Zhao, et al., Environ. Sci. Technol. 57 (2023) 14071–14081.
[23] S. Goyal, M.S. Shaharun, C.F. Kait, et al., J. Phys.: Conf. Ser. 1123 (2018) 012062.
[24] Y. Yao, H. Chen, J. Qin, et al., Water Res. 101 (2016) 281–291.
[25] N. Zhang, E.P. Tsang, K. Wang, et al., Sci. Total Environ. 764 (2021) 142813.
[26] X. Song, Y. Shi, Z. Wu, et al., Appl. Catal. B 340 (2024) 123240.
[27] H. Zhang, C. Zhou, H. Zeng, et al., J. Hazard. Mater. 395 (2020) 122613.
[28] P. Duan, J. Pan, W. Du, et al., Appl. Catal. B 299 (2021) 120714.
[29] C. Guan, J. Jiang, S. Pang, et al., Environ. Sci. Technol. 51 (2017) 10718–10728.
[30] L. Yang, Z. Xiong, J. Li, et al., Chem. Eng. J. 444 (2022) 136623.
[31] Y. Liu, W. Miao, X. Fang, et al., Chem. Eng. J. 380 (2020) 122584.
[32] Y. Hong, H. Zhou, Z. Xiong, et al., Chem. Eng. J. 391 (2020) 123604.
[33] H. Zhou, J. Peng, J. Li, et al., Water Res. 188 (2021) 116529.
[34] Z. Yang, J. Qian, C. Shan, et al., Environ. Sci. Technol. 55 (2021) 14494–14514.
[35] T. Zhang, Y. Chen, Y. Wang, et al., Environ. Sci. Technol. 48 (2014) 5868–5875.
[36] H. Zhou, J. Peng, X. Duan, et al., Environ. Sci. Technol. 57 (2023) 3334–3344.
[37] Y. Wang, H. Xia, K. Sun, et al., Chem. Eng. J. 304 (2016) 1000–1008.
[38] X. Du, Y. Zhang, F. Si, et al., Chem. Eng. J. 356 (2019) 178–189.
[39] L. Wang, H. Xu, N. Jiang, et al., Environ. Sci. Technol. 54 (2020) 4686–4694.
[40] S. Wang, J. Tian, Q. Wang, et al., Appl. Catal. B 256 (2019) 117783.
[41] X. Long, Z. Xiong, R. Huang, et al., Appl. Catal. B 317 (2022) 121716.
[42] Y. Lee, U. von Gunten, Water Res. 46 (2012) 6177–6195.
[43] P. Zhang, P. Zhou, J. Peng, et al., Water Res. 219 (2022) 118626.
[44] Y. Yu, C. Yu, Z. Wu, et al., Chem. Eng. J. 457 (2023) 141340.
[45] Y. Yu, Z. Xiong, B. Huang, et al., Environ. Int. 168 (2022) 107453.
[46] K. Yin, R. Wu, Y. Shang, et al., Appl. Catal. B 329 (2023) 122558.